Available online at www.eccomasproceedia.org
Eccomas Proceedia COMPDYN (2023) 1364-1379

ECCOMAS
Proceedia

COMPDYN 2023
9th ECCOMAS Thematic Conference on
Computational Methods in Structural Dynamics and Earthquake Engineering
M. Papadrakakis, M. Fragiadakis (eds.)
Athens, Greece, 12-14 June 2023

OPTIMAL TOPOLOGICAL DESIGN OF STRUCTURES SUBJECTED TO NON-STATIONARY STOCHASTIC EXCITATIONS

Giulia Angelucci[1], Giuseppe Quaranta[2], Fabrizio Mollaioli[1]

[1] Department of Structural and Geotechnical Engineering, Sapienza University of Rome
Via Gramsci 53, 00197 Rome, Italy
e-mail: {giulia.angelucci, fabrizio.mollaioli}@uniroma1.it

[2] Department of Structural and Geotechnical Engineering, Sapienza University of Rome
Via Eudossiana 18, 00184 Rome, Italy
e-mail: {giuseppe.quaranta}@uniroma1.it

Abstract

Topology optimization procedures are emerging as powerful tools for guiding the identification of enhanced structural systems that can meet the minimum weight and cost requirements while ensuring superior structural performances. Within this framework, it is too evident that the elaboration of efficient design solutions requires an accurate prediction of the structural response induced by natural or man-made hazards. In case of structural systems located within earthquake-prone areas, for instance, disregarding the aleatory uncertainty of the seismic excitation would lead to sub-optimal and poorly performing systems, or even to design solutions that do not comply with safety requirements. Unfortunately, handling with uncertainties into topology optimization problems is really challenging because the satisfactory description of the design domain requires a very large design vector. Hence, this work illustrates a novel approach for the optimal design of lateral resisting systems in multi-story buildings subjected to seismic ground motions. Herein, the base excitation is simulated as fully non-stationary stochastic process and the topology optimization problem is formulated in such a way to minimize the dynamic compliance of linear elastic multi-story buildings via the Solid Isotropic Material with Penalization approach. In order to accommodate the use of efficient gradient-based optimization algorithms, the sensitivity of the dynamic responses is performed analytically by means of an approximated procedure that involves sub-assemblies of the whole design domain. Stability and effectiveness of the proposed optimum design procedure are demonstrated via numerical examples where the non-stationary properties of the stochastic excitations are tuned to mimic different soil conditions.

Keywords: Lateral bracing system, Seismic design, Stochastic excitation, Topology optimization, Non-stationary random vibrations.

ISSN:2623-3347
Peer-review under responsibility of the organizing committee of COMPDYN 2023.
doi: 10.7712/120123.10482.20610

1 INTRODUCTION

The superior ability of structural topology optimization in identifying high-performance, yet cost-effective design solutions for load-resisting structural systems is nowadays well acknowledged.

A valuable support has been provided by past research in recognizing the robustness of automated optimization procedures under equivalent static loading conditions [1-4]. However, it is well understood that the performance reliability of optimized designs closely depends on the accurate prediction of the loading conditions to which structural systems might be exposed during their lifetime. In the topology optimization of earthquake-resistant structures, this imposes to properly account for the variability of the structural responses over the seismic scenario, which can be coherently simulated as a stochastic process. In this sense, recent efforts are directed towards a more rational description of the inherent randomness affecting many natural hazards and its incorporation into topology optimization frameworks.

Zhu et al. [5] investigated the minimization of the variance of framed systems under stationary stochastic ground motion by comparing time domain, frequency domain and state-space methods. In Angelucci et al., the topology optimization under stationary stochastic excitation was explored via random vibration theory considering both energy-based [6] and displacement-based [7] performance objectives. Under the same assumptions, Gomez and Spencer [8] developed an efficient adjoint method to accommodate the use of gradient-based approaches for the solution of optimization problems in stationary conditions.

Most of the research conducted so far on the optimized response of lateral resisting topologies subjected to random vibrations assumes a stationary excitation. However, this simplification can poorly reproduce the main features of actual ground motions as it does not allow adequate consideration of the time variation of amplitude and frequency content.

In the case of fixed topologies, optimization procedures driven by nonstationary stochastic excitations are relatively well established [9-11], but the same cannot be said for topology optimization. The main challenge in developing such a framework can be traced back to how topology optimization problems are inevitably characterized by large design variable vectors, which are required to adequately describe the design domain.

The combination with nonstationary dynamic loads further complicates the calculation of the stochastic response sensitivities with respect to each design variable and at each interval of the ground motion time window. This ultimately makes a crude use of the direct differentiation method impracticable, while dealing with nonstationary random vibrations renders the implementation of the adjoint method unviable.

To overcome this difficulty, a numerical strategy based on local approximations has been proposed by Angelucci et al. [12] to facilitate the computation of the required derivatives of the structural response covariances. Based on the findings emerged in this previous work, further insights are presented here for the optimal design of lateral resisting systems in multi-story buildings subjected to fully nonstationary stochastic ground motions.

The framework directly incorporates the stochastic nature of the seismic excitation into the topology optimization procedure. The variances of the responses are employed to construct the objective function aimed at minimizing the stochastic dynamic compliance of the structural system. An illustrative example is presented to demonstrate the applicability as well as the stability and robustness of the proposed optimization approach.

2 STOCHASTIC OPTIMIZATION PROBLEM

The formulation of the topology optimization under fully nonstationary stochastic excitations is discussed in this section. The optimization problem is posed to minimize the stochastic dynamic compliance of the structural system to attain the optimal material distribution of the density variables within the design domain. This is in line with the standard formulation developed so far in the literature, e.g. within static deterministic settings [3,4] or stationary stochastic dynamic settings [7], also facilitating the comparison with prior benchmark studies. Herein, the seismic ground motion is simulated as a filtered white noise, and the state-space representation of the structural system dynamics and the excitation model is employed.

2.1 Stochastic excitation model

The seismic ground motion $\ddot{x}_g$ is modeled as a white Gaussian noise filtered through the Clough-Penzien filter model and written in the state-space form as follows:

$$\ddot{x}_g = \mathbf{a}_p{}^{\mathrm{T}}\mathbf{y}_p \tag{1}$$

$$\dot{\boldsymbol{y}}_p = \mathbf{D}_p\mathbf{y}_p + \mathbf{v}_p W \tag{1b}$$

where $\mathbf{y}_p$ is the state vector for the excitation filter; $\mathbf{a}_p$, $\mathbf{D}_p$ and $\mathbf{v}_p$ represent the characteristics of the excitation:

$$\mathbf{y}_p = \{x_p \;\; \dot{x}_p \;\; x_k \;\; \dot{x}_k\}^{\mathrm{T}} \tag{2a}$$

$$\mathbf{a}_p = \{-\omega_p^2 \;\; -2\xi_p\omega_p \;\; \omega_k^2 \;\; -2\xi_k\omega_k\}^{\mathrm{T}} \tag{2b}$$

$$\mathbf{D}_p = \begin{bmatrix} 0 & 1 & 0 & 0 \\ -\omega_p^2 & -2\xi_p\omega_p & \omega_k^2 & 2\xi_k\omega_k \\ 0 & 0 & 0 & 1 \\ 0 & 0 & -\omega_k^2 & -2\xi_k\omega_k \end{bmatrix} \tag{2c}$$

$$\mathbf{v}_p = \{0 \;\; 0 \;\; 0 \;\; -\varphi\}^{\mathrm{T}} \tag{2d}$$

where ω_p and ξ_p, ω_k and ξ_k are the dominant circular frequency and dominant damping ratio of the Kanai-Tajimi and Clough-Penzien filters, respectively. The parameter φ represents the amplitude modulation function.

Under the assumption of fully nonstationary seismic excitation, both ω_k and φ are assumed as time-dependent functions in order to account for the non-stationarity in frequency content and amplitude of the seismic ground motion, respectively.

W is a zero-mean white Gaussian noise having constant power spectral density S_0, evaluated as a function of the peak ground acceleration $\ddot{x}_g^{\max}$ according to the relationship proposed by Liu et al. [13]:

$$S_0 = \frac{(\ddot{x}_g^{\max})^2}{\delta^2 \left[\pi\, \omega_k \left(2\xi_k + \frac{1}{2\xi_k}\right)\right]} \tag{3}$$

where δ = 2.80 denotes the peak factor. In case of fully nonstationary seismic excitation, the constant value of S_0 is preserved by introducing a constant value of the dominant circular frequency ω_k.

2.2 Structural model dynamics

The structure is assumed to be a linear elastic time invariant system with N_f degrees of freedom resulting from the finite element discretization of the design domain. The motion equation of the structural system subjected to the horizontal seismic excitation within the time window [0, T] can be written in the following state-space form:

$$\dot{\mathbf{y}}_\mathbf{s} = \mathbf{A}_\mathrm{s}\, \mathbf{y}_\mathrm{s} + \mathbf{H}_\mathrm{p}\, \mathbf{y}_\mathrm{p} \tag{4}$$

where $\mathbf{y}_s$ is the $2N_f \times 1$ state vector, i.e. $\mathbf{y}_s = \{\mathbf{u}\ \dot{\mathbf{u}}\}^\mathrm{T}$, while $\mathbf{H}_p$ and $\mathbf{A}_s$ are defined as follows:

$$\mathbf{A}_s = \begin{bmatrix} \mathbf{0}_{N_f} & \mathbf{I}_{N_f} \\ -\mathbf{M}^{-1}\mathbf{K} & -\mathbf{M}^{-1}\mathbf{C} \end{bmatrix} \tag{5a}$$

$$\mathbf{H}_p = \begin{bmatrix} \mathbf{0}_{N_f \mathrm{x} 4} & -\mathbf{r}\mathbf{a}_p^\mathrm{T} \end{bmatrix}^\mathrm{T} \tag{5b}$$

where **r** is the incidence vector; **M** and **K** are the global mass and stiffness matrices of the structure, respectively. The linear viscous damping matrix **C** of the structural system is formulated as a linear combination of the mass and stiffness matrices according to the Rayleigh damping model.

2.3 Covariance of the structural responses

An augmented state vector **y** is defined as $\mathbf{y} = \{\mathbf{y}_s\ \ \mathbf{y}_p\}^\mathrm{T}$ to yield an assembled representation of the structural system and the filtered excitation, as follows:

$$\dot{\mathbf{y}} = \mathbf{A}\, \mathbf{y} + \mathbf{f} \tag{6}$$

where

$$\mathbf{A} = \begin{bmatrix} \mathbf{A}_s & \mathbf{H}_p \\ \mathbf{0}_{4\mathrm{x}2N_f} & \mathbf{D}_p \end{bmatrix} \tag{7a}$$

$$\mathbf{f} = \begin{Bmatrix} \mathbf{0}_{2N_f \mathrm{x} 1} \\ \mathbf{v}_p W \end{Bmatrix} \tag{7b}$$

By applying the mean value operator $\mathbb{E}[\cdot]$, the corresponding covariance matrix of the structural responses $\mathbf{R}$ is defined as:

$$\mathbf{R} = \mathbb{E}[\mathbf{y}\mathbf{y}^{\mathrm{T}}] = \begin{bmatrix} \mathbf{R}_{\mathbf{y}_s\mathbf{y}_s} & \mathbf{R}_{\mathbf{y}_s\mathbf{y}_p} \\ \mathbf{R}_{\mathbf{y}_p\mathbf{y}_s} & \mathbf{R}_{\mathbf{y}_p\mathbf{y}_p} \end{bmatrix} \tag{8}$$

which, in turn, can be determined through the solution of the following Lyapunov equation in nonstationary conditions:

$$\mathbf{A}\mathbf{R} + \mathbf{R}\mathbf{A}^{\mathrm{T}} + \mathbf{B} = \dot{\mathbf{R}} \tag{9}$$

where $\mathbf{B}$ is a null matrix except for the element whose index is $(2N_f + 4, 2N_f + 4)$, which is equal to $2\pi S_0$.

In order to solve Eq. (9), the time window $[0, T]$ of the base excitation is arranged as a discrete sequence of evenly spaced time instants with constant time step Δt. If a linear variation of $\dot{\mathbf{R}}$ is supposed within each time interval, then the original Lyapunov equation can be conveniently converted into the following stationary form at each time step:

$${}^{i+1}\overline{\mathbf{A}}\ {}^{i+1}\mathbf{R} + {}^{i+1}\mathbf{R}\ {}^{i+1}\overline{\mathbf{A}}^{\mathrm{T}} + {}^{i+1}\overline{\mathbf{B}} = \mathbf{0}_{2N_f+4} \tag{10}$$

where

$${}^{i+1}\overline{\mathbf{A}} = \frac{1}{2}\left(-\mathbf{I}_{2N_f+4} + \Delta t\,{}^{i+1}\mathbf{A}\right) \tag{11a}$$

$${}^{i+1}\overline{\mathbf{B}} = \left(\mathbf{I}_{2N_f+4} + \frac{1}{2}\Delta t\ {}^{i}\mathbf{A}\right)\ {}^{i}\mathbf{R} + \frac{1}{2}\Delta t\ {}^{i}\mathbf{R}\ {}^{i}\mathbf{A}^{\mathrm{T}} + \frac{1}{2}\Delta t\left({}^{i+1}\mathbf{B} + {}^{i}\mathbf{B}\right) \tag{11b}$$

By solving Eq. (10) recursively at each time instant, the covariance of the nonstationary structural responses can finally be calculated through numerical approximation (i.e., via trapezoidal numerical integration).

2.4 Optimum design under nonstationary seismic excitation

Once the covariance sub-matrix of the structural displacements $\mathbf{R}_{\mathbf{uu}}$ (i.e., the square block of size $N_f \times N_f$) is extracted from the complete covariance matrix of the system response defined in Eq. (8), the objective function f of the optimization problem reads:

$$f = \mathbb{E}\left[\int_0^T \mathbf{u}^{\mathrm{T}}\mathbf{K}\mathbf{u}\ \mathrm{d}t\right] = \int_0^T \mathbf{r}^{\mathrm{T}}(\mathbf{K} \otimes \mathbf{R}_{\mathbf{uu}})\mathbf{r}\ \mathrm{d}t \tag{12}$$

with

$$\mathbf{R}_{\mathbf{y}_s\mathbf{y}_s} = \begin{bmatrix} \mathbf{R}_{\mathbf{uu}} & \mathbf{R}_{\mathbf{u\dot{u}}} \\ \mathbf{R}_{\mathbf{\dot{u}u}} & \mathbf{R}_{\mathbf{\dot{u}\dot{u}}} \end{bmatrix} \tag{13}$$

where $\otimes$ is the term-by-term product. Hence, the topology optimization problem under fully nonstationary stochastic excitations can be formulated as follows:

$$\begin{aligned} \min_{\boldsymbol{\rho}} : \quad & \int_0^T \mathbf{r}^{\mathrm{T}} \left(\mathbf{K} \otimes \mathbf{R}_{\mathbf{uu}}\right) \mathbf{r} \, \mathrm{d}t \\ \text{s.t.} : \quad & \sum_{e=1}^{N_f} V_e \leq V_{\max} \\ & \boldsymbol{\rho}_{\min} \leq \boldsymbol{\rho} \leq \boldsymbol{\rho}_{\max} \end{aligned} \tag{14}$$

where V_e is the volume of the eth finite element and $\boldsymbol{\rho}$ represents the set of design variables with lower and upper bounds $\boldsymbol{\rho}_{\min}$ and $\boldsymbol{\rho}_{\max}$, respectively. The constraint function in Eq. (14) enforces a volume reduction in the final solution so as not to exceed the specified threshold value of $V_{\max}$.

In order to ensure well-posedness as well as existence and uniqueness of the solution for the topology optimization problem, the Solid Isotropic Material with Penalization (SIMP) approach [14] is adopted in this work. Consistently, the design variables are the artificial densities of the elements whose material properties (i.e. the local mass and stiffness matrices) are expressed as material interpolation functions such that intermediate properties are penalized by using a heuristic power-law. Global matrices are finally assembled introducing the standard finite element operator, as follows:

$$\mathbf{K}(\boldsymbol{\rho}) = \bigwedge_{e=1}^{N_f} \rho_e{}^p \mathbf{K}_e^0 \tag{15a}$$

$$\mathbf{M}(\boldsymbol{\rho}) = \bigwedge_{e=1}^{N_f} \rho_e{}^q \mathbf{M}_e^0 \tag{15b}$$

where $\mathbf{M}_e^0$ and $\mathbf{K}_e^0$ are the mass and stiffness matrices of the eth finite element of the design domain with solid material, respectively. The related penalization factors are here assumed to be $q = 1$ and $p = 3$, since these values generally provide good convergence properties towards the binary solution. In agreement with the Rayleigh's model, the viscous damping matrix can also be re-arranged to be design-dependent, as follows:

$$\mathbf{C}(\boldsymbol{\rho}) = a_0 \, \mathbf{M}(\boldsymbol{\rho}) + a_1 \, \mathbf{K}(\boldsymbol{\rho}) \tag{15c}$$

whereas a_0 and a_1 are two positive constants calculated by imposing that the damping ratio is the same for the first two modes of the structure.

3 SOLUTION METHOD

3.1 Sensitivity analysis

A numerical gradient-based procedure is typically preferred to solve optimal material distribution problems in the form given in Eq. (14). Thus, updating each element-wise density involves the evaluation of the sensitivities of both objective and constraint functions with respect to the design variables. While the calculation of the cost gradient is straightforward, the derivative of the objective function reads:

$$\frac{\partial f}{\partial \rho_e} = \int_0^T \mathbf{r}^{\mathrm{T}} \left(\frac{\partial \mathbf{K}}{\partial \rho_e} \otimes \mathbf{R}_{\mathrm{uu}} \right) \mathbf{r} \, dt + \int_0^T \mathbf{r}^{\mathrm{T}} \left(\mathbf{K} \otimes \frac{\partial \mathbf{R}_{\mathrm{uu}}}{\partial \rho_e} \right) \mathbf{r} \, dt \tag{16}$$

It is easily recognized that the global stiffness matrix is an explicit function of the design variables according to the material interpolation scheme provided in Eq. (15a). Thus, the term $\partial \mathbf{K}/\partial \rho_e$ can effortlessly be revised as:

$$\frac{\partial \mathbf{K}}{\partial \rho_e} = \bigwedge_{e=1}^{N_f} \frac{\partial \mathbf{K}_e}{\partial \rho_e} = \bigwedge_{e=1}^{N_f} p {\rho_e}^{p-1} \mathbf{K}_e^0 \tag{17}$$

On the other hand, the displacement covariance matrix implicitly accommodates the design variables through the combination of the mass and stiffness structural matrices, as occurs in Eq. (10). If a direct differentiation approach is employed, the term $\partial \mathbf{R}_{\mathrm{uu}}/\partial \rho_e$ can be extracted conveniently from the derivative of $\mathbf{R}$ with respect to ρ_e, once the following associate stationary Lyapunov equation is solved:

$${}^{i+1}\bar{\mathbf{A}} \frac{\partial {}^{i+1}\mathbf{R}}{\partial \rho_e} + \frac{\partial {}^{i+1}\mathbf{R}}{\partial \rho_e} {}^{i+1}\bar{\mathbf{A}}^{\mathrm{T}} + {}^{i+1}\bar{\bar{\mathbf{B}}} = \mathbf{0}_{2N_f+4} \tag{18}$$

where

$${}^{i+1}\bar{\bar{\mathbf{B}}} = \frac{1}{2}\Delta t \frac{\partial {}^{i+1}\mathbf{A}}{\partial \rho_e} {}^{i+1}\mathbf{R} + \frac{1}{2}\Delta t \, {}^{i+1}\mathbf{R} \frac{\partial {}^{i+1}\mathbf{A}^{\mathrm{T}}}{\partial \rho_e} + \frac{\partial {}^{i+1}\bar{\bar{\mathbf{B}}}}{\partial \rho_e} \tag{19}$$

Regardless of the non-stationarity of the seismic excitation, it is noted that:

$$\frac{\partial {}^{i+1}\mathbf{A}}{\partial \rho_e} = \begin{bmatrix} \dfrac{\partial \mathbf{A}_s}{\partial \rho_e} & \mathbf{0}_{2N_f \times 4} \\ \mathbf{0}_{4 \times 2N_f} & \mathbf{0}_4 \end{bmatrix} \tag{20a}$$

with

$$\frac{\partial \mathbf{A}_s}{\partial \rho_e} = \begin{bmatrix} \mathbf{0}_{N_f} & \mathbf{0}_{N_f} \\ \mathbf{M}^{-1}\dfrac{\partial \mathbf{M}}{\partial \rho_e} \; \mathbf{M}^{-1}\mathbf{K} - \mathbf{M}^{-1}\dfrac{\partial \mathbf{K}}{\partial \rho_e} & \mathbf{M}^{-1}\dfrac{\partial \mathbf{M}}{\partial \rho_e} \; \mathbf{M}^{-1}\mathbf{C} - \mathbf{M}^{-1}\dfrac{\partial \mathbf{C}}{\partial \rho_e} \end{bmatrix} \tag{20b}$$

The derivatives of the mass and damping matrices with respect to the design variables are determined in agreement with the SIMP approach, likewise to what is discussed for the stiffness matrix in Eq. (17). A complete derivation of the sensitivity analysis for the covariance matrix is provided in Angelucci et al. [12], to which the reader is referred for further details.

Once Eqs. (10) and (16) are solved at each time instant, the exact gradient of the objective function with respect to the *e*th variable can be finally computed via trapezoidal numerical integration. Apparently, these operations must be repeated for all the variables of the design domain until the convergence of the topology optimization problem is attained.

3.2 Approximated sensitivity of stochastic response

It is clearly understood that the solution procedure based on the exact, direct differentiation method is neither computationally viable nor memory affordable when dealing with the topology optimization of large, or fine-meshed, domains under fully nonstationary conditions. Since accomplishing this task at global level requires prohibitive time consumption, an alternative numerical approach is herein introduced to improve the efficiency of the optimization framework.

By virtue of the SIMP scheme, the material density of each finite element is regarded as an independent design variable. The other structural properties are assembled as continuous functions with respect to density by interpolating the respective values for each artificial material. This suggests that the gradient of the stiffness matrix in Eq. (17) is null except for the degrees of freedom of the *e*th finite element for which the derivative is computed. Regardless of the size of the design domain considered, the following relationship always holds: $\partial \mathbf{K} / \partial \rho_e = \partial \mathbf{K}_e / \partial \rho_e$. Thus, the first addend in Eq. (16) can be simplified accordingly:

$$\mathbf{r}^{\mathrm{T}} \left(\frac{\partial \mathbf{K}}{\partial \rho_e} \otimes \mathbf{R}_{\mathbf{uu}} \right) \mathbf{r} = \mathbf{r}_{\Omega_e}^{\mathrm{T}} \left(\frac{\partial \mathbf{K}_{\Omega_e}}{\partial \rho_e} \otimes \mathbf{R}_{\mathbf{uu},\,\Omega_e} \right) \mathbf{r}_{\Omega_e} \tag{19}$$

where $\mathbf{r}_{\Omega_e}$ and $\mathbf{R}_{\mathbf{uu},\,\Omega_e}$ are the incidence vector and the covariance matrix of the structural displacements, respectively, computed considering solely the degrees of freedom of the *e*th finite element of the design domain Ω. This conversion allows to deal with reduced-order matrices, which significantly expedite the calculation of the derivatives within the time discretization.

Though the same transformation does not strictly apply to the gradient of the covariance matrix, it is supposed here that it approximately holds for a sub-assembly including the *e*th finite element with respect to which the derivative is performed and some finite elements within its neighborhood. Therefore, the following relationship is herein expediently assented:

$$\frac{\partial \mathbf{R}_{\mathbf{uu}}}{\partial \rho_e} \approx \bigwedge_{e \in \Pi_e} \frac{\partial \mathbf{R}_{\mathbf{uu},\Pi_e}}{\partial \rho_e} \tag{20}$$

where $\Pi_e \subseteq \Omega$ is the subset of the optimizable domain, at least represented by the single *e*th finite element.

Once the sub-assembly is identified, the explicit, exact derivatives are analytically computed through direct differentiation of the related Lyapunov equation under nonstationary conditions. It is too evident that the least computationally demanding approximation is accomplished

when the sub-assembly degenerates into the single finite element. Consistently, the second addend in Eq. (16) can be reformulated as:

$$\mathbf{r}^{\mathrm{T}}\left(\mathbf{K}\otimes\frac{\partial\mathbf{R}_{\mathbf{uu}}}{\partial\rho_e}\right)\mathbf{r}\approx\mathbf{r}_{\Omega_e}^{\mathrm{T}}\left(\mathbf{K}\otimes\frac{\partial\mathbf{R}_{\mathbf{uu},\Omega_e}}{\partial\rho_e}\right)\mathbf{r}_{\Omega_e} \tag{21}$$

Because the approximation tends to the exact solution as the sub-assembly approaches the design domain (i.e. $\Pi_e \rightarrow \Omega$), the element-wise scheme in Eq. (21) is likely to lead to the highest error in performing the derivatives. If needed, the accuracy of the approximation can be improved by expanding the subdomain size to specifically include additional finite elements within the neighborhood. However, it should be noted that beyond a certain extent of the sub-assembly, the results might not undergo appreciable improvements to the detriment of the calculation cost.

3.3 Validation of sub-assembly approach

Within the framework of the proposed methodology, some computationally efficient definitions of the sub-assembly Π_e are presented and their accuracy in approximating the exact gradient of the objective function is discussed.

As a running example, the topology optimization of a simple 5 m x 5 m continuous design domain with fixed base is considered. Symmetry constraints are enforced about the centerline. Young's modulus of 21 GPa and density of 2,400 kg/m^3 are used to describe the material properties of the system. It is assumed that the mass is concentrated at both upper corners and calculated considering dead and live loads equal to 7.0 kN/m^2 and 2.0 kN/m^2, respectively. The volume fraction is set to 30% of the overall volume of the domain, and a density filter with radius equal to 0.3 m is employed.

Because the calculation of the exact derivatives of the covariance matrix with respect to each design variable at each time step would be prohibitive in the case of nonstationary excitation, stationary conditions are initially considered. It should be emphasized that such a simplification does not compromise the consistency of the validation since the proposed method applies indiscriminately to both the stationary and fully nonstationary cases. The ground motion is thus modeled as a filtered white Gaussian noise with peak ground acceleration equal to 0.3 g, and constant filter parameters specified as follows: $\xi_p = \xi_k = 0.6$, $\omega_p = 1.5$ rad/s and $\omega_k = 15$ rad/s.

The approximated gradient evaluation is performed according to the proposed procedure by considering the whole domain (global level) and a single finite element only (local level), as shown in Figure 1. A mesh refinement of the discretized domain is considered to evade numerical mesh-dependency instabilities. Divergences in the attainment of the optimal solution are monitored by gradually decreasing the size of the sub-assembly, systematically checking the demanding computational cost, approximation of the objective sensitivities, and final material distribution. Because the calculation of the exact objective sensitivities at the global level, i.e. when Π_e coincides with Ω, does not include any approximation, it is assumed as an error measure for the proposed methodology.

Figure 2 shows minimal discrepancies of the sensitivity values of the objective function obtained by means of the direct procedure and the proposed approximation, which gradually reduce as the number of elements included in the sub-domain converges to the complete optimizable domain. However, on average these disagreements are reasonably small so as not to alter the final topological results, as displayed in Figure 3. This result is consistent with the

initial mechanical interpretation: variations of the *e*th design variable are almost insensitive to the response contribution of elements far enough from the *e*th element itself. In this regard it should be emphasized that the accuracy on the calculation of the derivatives of the stiffness matrix is independent on the number of elements included in the sub-domain, as provided in Eq. (19). Thus, the relative errors on the updating variables are merely attributable to the evaluation of the derivatives of the covariance matrix given in Eq. (21), which determines the goodness of the approximation for both topologies and sensitivities. Moreover, the gradient vector of the objective function at a current point only contributes to identify the search directions towards the optimal solution (i.e. the global minimum of the performance function). Because the derivatives of the objective function has no other physical meaning and the final topologies at the end of the optimization procedure are qualitatively the same, it is asserted that small differences produced by the approximation models in the sensitivity analysis do not affect the optimal material distribution within the domain.

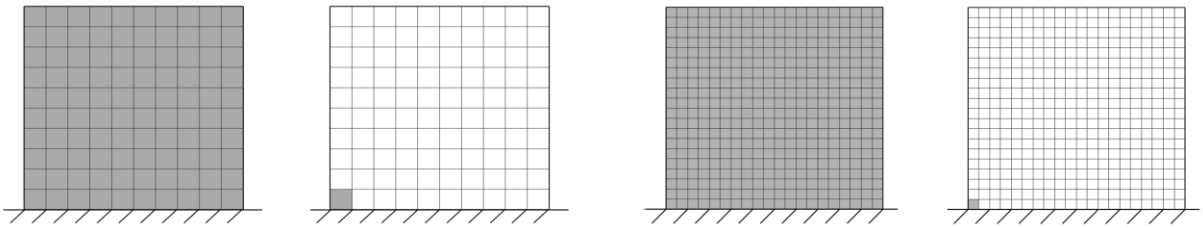

Figure 1. Layout for the optimizable domain consisting of Q4 finite elements with mesh size of 0.50 m × 0.50 (a, b) and mesh size of 0.25 m × 0.25 m (c, d) under stationary base motion. Sub-assembly considering the whole domain (a, c) and a subassembly with a single element only (b, d).

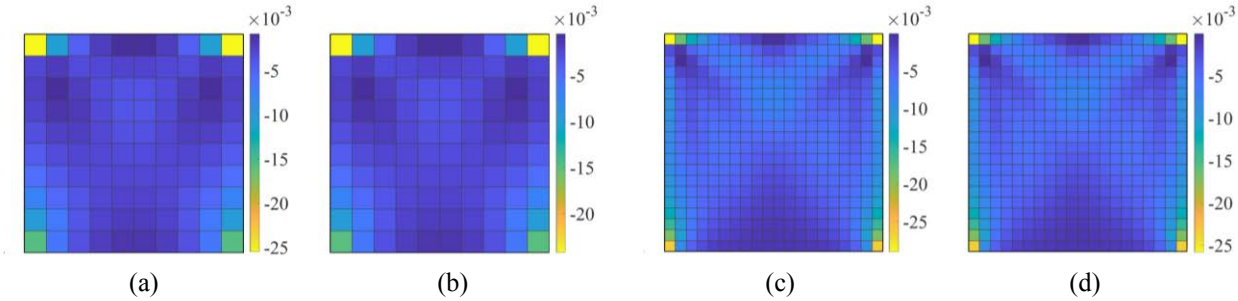

Figure 2. Sensitivity analysis of the objective function for the optimizable domain consisting of Q4 finite elements with mesh size of 0.50 m × 0.50 (a, b) and mesh size of 0.25 m × 0.25 m (c, d) under stationary base motion. Sub-assembly considering the whole domain (a, c) and a subassembly with a single element only (b, d).

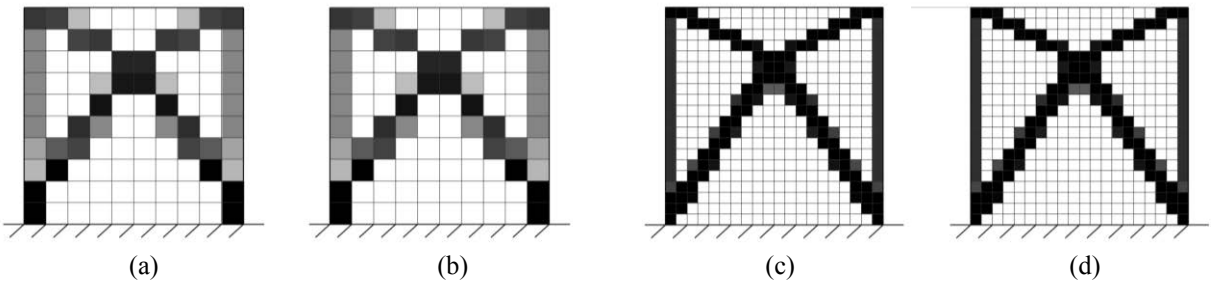

Figure 3. Final material distribution for the optimizable domain consisting of Q4 finite elements with mesh size of 0.50 m × 0.50 (a, b) and mesh size of 0.25 m × 0.25 m (c, d) under stationary base motion. Sub-assembly considering the whole domain (a, c) and a subassembly with a single element only (b, d).

The applicability of the proposed methodology remains numerically valid also in the case of nonstationary base motion.

The improvement in the accuracy of the approximate gradient evaluation is estimated by expanding the size of the sub-domain Π_e in such a way to include other finite elements within the neighborhood in addition to the eth finite element for which the derivative is calculated. Sub-assemblies with 8 neighborhood finite elements and 4 neighborhood finite elements are considered as intermediate cases to reduce the error attributable to the computation of the sensitivities. Figure 4 (a) provides the computational cost demanded by the first 10 iterations of the optimization procedure in case of fully nonstationary excitation. The results in Figure 4 (b) reveal that expanding the element neighborhood produces little effect on the sensitivities of the objective function while the root-mean-square error reduces with the mesh size. These findings confirm that the smallest sub-assembly, consisting of a single finite element, is good enough to attain a satisfactory accuracy of the sensitivities with least computational effort.

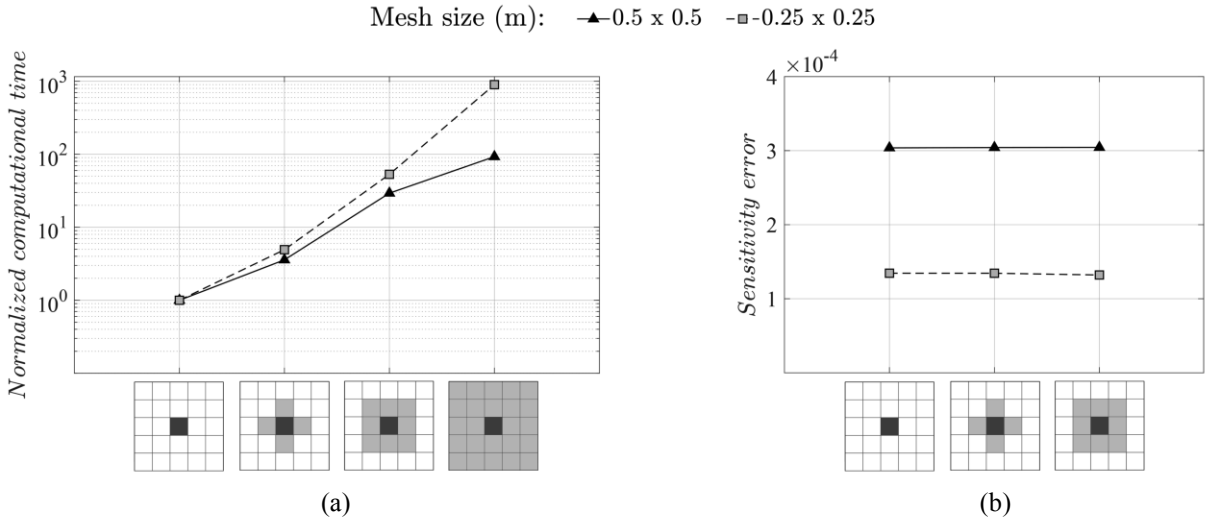

Figure 4. Optimizable domain consisting of Q4 finite elements 0.50 m × 0.50 m and 0.25 m × 0.25 m under nonstationary base motion. Computation time demands normalized with respect to the elaboration time required for the sub-assembly including the single finite element only (a). Root-mean-square error of the sensitivity of the objective function (b).

4 NUMERICAL APPLICATION

In this section, the proposed approximation approach is applied to identify the optimal lateral bracing system of a multi-story building subjected to seismic ground motion excitation. In detail, the optimal material distribution within the design domain is attained by minimizing the stochastic compliance of the structural system while imposing a constraint on the allowable volume, as given in Eq. (14). The gradient of the objective function is here computed for a sub-assembly including a single finite element only, since the numerical validation provided in Section 3 has confirmed that it practically reproduces exact optimized topologies.

4.1 Input seismic excitation

In this work, the non-stationarity in both amplitude and frequency content of the seismic excitation is properly taken into account according to the mathematical model proposed by Fan and Ahmadi [15]. The benchmark building is located at the stiff soil in El Centro.

Figure 5 (a) shows the smooth standard deviation function e of the record amplitude as a function of time. The first 29.8 s of the accelerogram, which contain 98% of the energy, are considered representative the strong ground motion of the El Centro earthquake [15].

The non-stationarity in amplitude of the stochastic seismic ground motion is simulated by means of the modulation function proposed by Jennings et al. [16]. Consistently, the envelope function ϕ is defined for three time intervals: a parabolically increasing branch, a plateau peak region (i.e. the strong motion phase) and an exponentially decaying phase regulated by a shape parameter of 0.5. The amplitude envelope function for the firm soil is shown in Figure 5 (b), together with the starting and ending time instants denoting the strong-motion phase.

Station	Soil type	ω_k	ξ_k	ω_p	ξ_p	PGA
El Centro	Firm	19.0 rad/s	0.65	2.0 rad/s	0.6	0.2 g

Table 1. Constant parameters of the nonstationary stochastic excitation process.

The non-stationarity of the frequency content is simulated by assuming that the dominant circular frequency ω_k is time-dependent and the expressions calibrated by Fan and Ahmadi for El Centro 1940 earthquake are considered. Constant values of the other filter parameters as well as the dominant frequency ω_k required to compute S_0 are specified in Table 1 in agreement with the estimates derived by Yeh and Wen [17] for El Centro ground motion. Figure 5 (c) shows the time-dependent dominant frequency ω_k adopted to simulate the non-stationarity of the frequency content (Fan & Ahmadi, 1991) and the constant value of ω_k employed to evaluate the power spectral density of the white Gaussian noise (Yen & Wen, 1990).

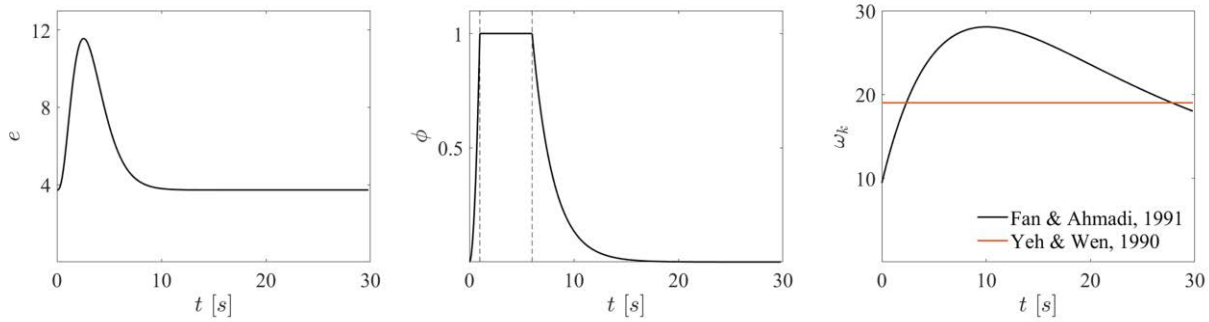

(a) (b) (c)

Figure 5. Variation of the amplitude standard deviation with time (a); non-stationary amplitude envelope function (b); non-stationary dominant frequency function and associated constant value for S_0 (c).

4.2 Five-story building

The topology optimization is performed for an ideal five-story planar building with height of 25 m and bay width of 5 m and floor slabs are placed every 5m. The external envelope of the building is assumed as a natural optimizable domain and discretized using 250 x 50 planar Q4 elements with uniform thickness of 0.1 m. The structure is idealized with fixed supports and symmetry constraints are enforced with respect to the vertical centerline.

To ensure a realistic description of the overall stiffness, the continuum domain is combined with a gravity framework which contributes in withstanding vertical and lateral loads. The presence of vertical members also helps reducing material concentration along the boundaries

of the final topologies with resulting better definition of the bracing schemes and clearer identification of the working points.

In addition to the load-bearing system, structural and non-structural floor components provide a significant and unavoidable source of mass, which triggers most of the inertial loading associated with the seismic excitation in multi-story buildings. Therefore, the assumption of mass concentrated at the floor levels is reasonably accepted and two master nodes with additional lumped mass of 4,000 kg are considered at each intersection of the framed system. It is understood that since inertial loads develop at the master nodes only, the complete system can be properly reduced to the degrees of freedom of the master nodes. This sub-structuring technique is especially beneficial in the case of stochastic topology optimization, where inversion and eigen analysis of large matrices are usually required to solve the Lyapunov equation and construct the covariance matrix.

To expediently relax the invariable components on the element update, both the secondary system and the mass sources are included within a non-optimizable domain so that their structural properties are not altered during the iterative optimization process. Moreover, since inertial loads develop at master nodes of the secondary system only and provided the assumption that the auxiliary perimeter framework is not included in the optimizable domain, the final topologies are independent of the particular location of the master nodes. This allows to arbitrarily choose the secondary system bounding the continuum domain as their definition does not interfere in determining the final designs.

4.3 Optimization results

The five-story building is analyzed under firm soil condition, and it was initially designed in such a way that its initial fundamental frequency (i.e., fundamental frequency corresponding to the initial volume fraction over the optimizable domain equal to 0.25) was as close as possible to the constant value of the dominant frequency of the soil (i.e., ω_k = 19 rad/s). Explicitly, the first natural frequency of the uniformly distributed domain is ω_1= 19.5 rad/s (with first natural period equal to 0.32 s). The domain discretization of the 5-story building is shown in Figure 6 (a) together with the optimized topologies obtained for nonstationary and stationary stochastic seismic ground motions (Figure 6 (b) and Figure 6 (c), respectively). The mode shapes of the first three vibration modes are also provided.

At the end of the optimization routines, the resulting natural frequency is 26.6 rad/s for the nonstationary ground motion and 22.6 rad/s for the stationary ground motion. In both models analyzed, the optimization procedure distributes most of the structural material in the lower levels first so as to increase the fundamental natural frequency of the system away from that of the ground. However, consistently with the outcomes of the modal analysis, the resulting topologies are qualitatively different. On the one hand, if a nonstationary condition is assumed to simulate the seismic ground motion, the structural layout arranges in a stiffer configuration with the formation of additional strengthening elements between the primary diagonals of the second module. On the other hand, when a stationary ground motion is considered, the lateral bracing system minimizes the dynamic compliance by thickening the diagonal members of the second module and adding two bracing arms at the third module.

A more comprehensive evaluation of the topological results can be appreciated by referring to the convergence histories of the objective functions and constraint functions in Figure 7 (a) and Figure 7 (b), respectively. The iterative histories confirm that the topology optimization problem based on the proposed sensitivity approach successfully converge towards optimal solutions. Particularly, the material distribution satisfying the volume constraint in the design domain is rapidly identified for both the analyzed cases. Further updating iterations are

required to attain the minimum dynamic compliance within the identified regions and eventually stabilize it. Although an identical material saving equal to 25% of the initial volume is observed, the two ground motion models lead to rather different compliance values. In detail, the iteration history of the objective function confirms that the nonstationary base excitation produces a stiffer geometric configuration for the lateral resisting system as the compliance settles on lower values than in the stationary case. These findings emphasize how substantially the ground motion modeling affect the final topologies. From this simple explanatory case-study, it is inferred the relevance of integrating topology optimization frameworks with sophisticated nonstationary simulations of stochastic excitations.

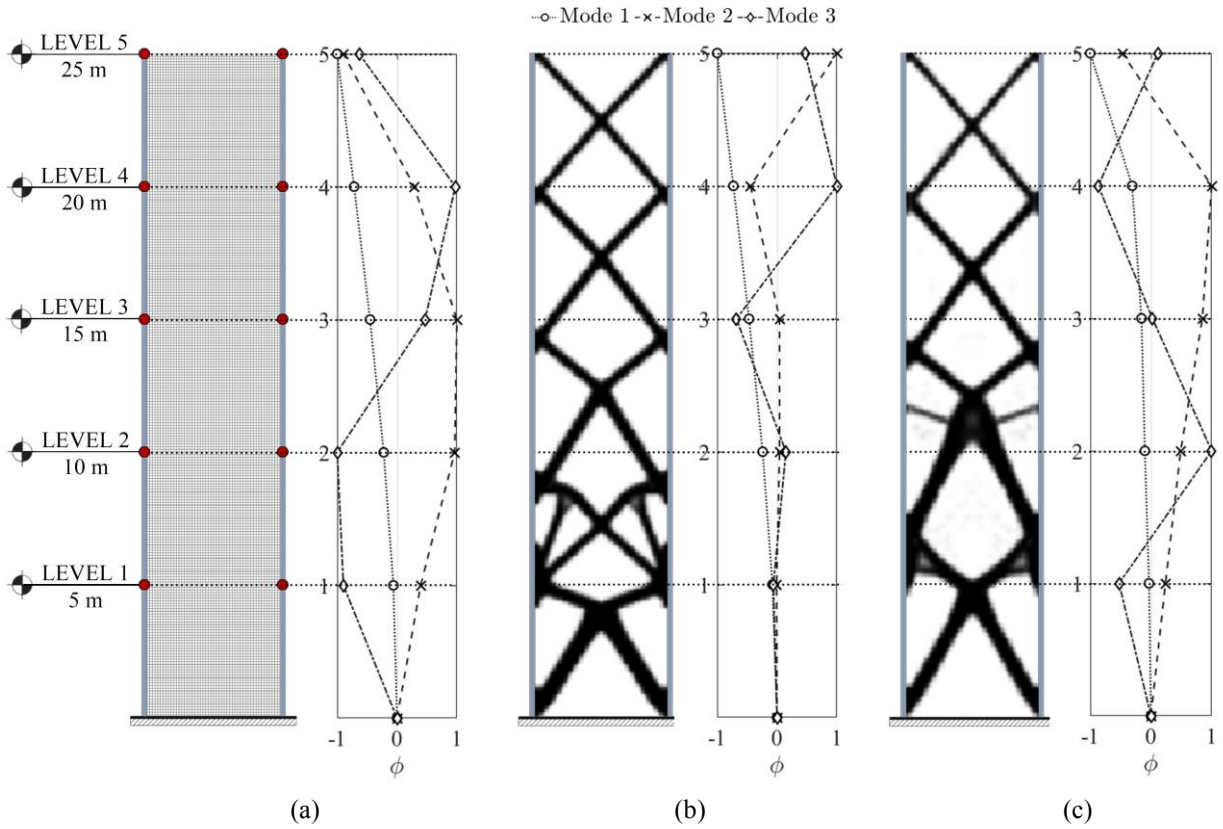

Figure 6. Topology optimization of a five-story building on firm soil: design domain (a) and final topologies under fully nonstationary condition (b) and stationary conditions (c).

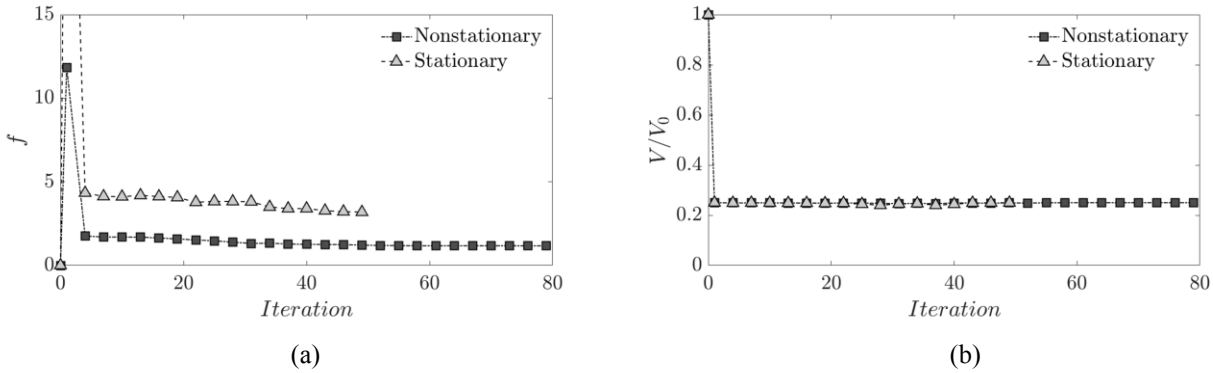

Figure 7. Convergence history of the optimization problem for a five-story building on firm soil: compliance (a) and volume (b).

5 CONCLUSIONS

It is well recognized that the time-varying parameters of the seismic ground motions can significantly affect the stochastic response of structures. This is even more stringent when reliable high-performance topologies are of interest. In this paper, a topology optimization framework has been proposed to find optimal lateral resisting systems of linear elastic multi-story buildings subjected to stochastic seismic ground motions. As typical of real earthquakes, a fully nonstationary excitation, accounting for the time-dependency of both intensity and frequency content, has been included in the optimization problem. The objective function is expressed by minimizing the compliance of the stochastic response based on the integration of the random vibration theory together with the renowned density-based approach. To accommodate the implementation of gradient-based solution algorithms, a sub-assembly approach is proposed for the calculation of the derivatives of the covariance matrix with respect to the design variables. Specifically, the gradient approximation based on a single finite element has been shown to drastically reduce the required computational effort while providing an excellent estimation of the sensitivities. A five-story building model has been employed to assess how time variation of the ground motion features affects the final optimal topologies. The results have demonstrated that whether the base excitation is simulated in stationary or non-stationary conditions has a significant impact on the geometrical arrangement of the final layouts, especially on brace-to-brace and brace-to-column nodes. It is concluded that neglecting the time variation of the intensity and frequency content of the input ground motion may lead to an underestimation of the lateral dynamic loading and, ultimately, to underperforming topologies.

REFERENCES

[1] L. L. Stromberg, A. Beghini, W. F. Baker, G. H. Paulino. Topology optimization for braced frames: combining continuum and beam/column elements. *Engineering Structures*, **37**, 106-124, 2012.

[2] G. Kazakis, I. Kanellopoulos, S. Sotiropoulos N. D. Lagaros. Topology optimization aided structural design: Interpretation, computational aspects and 3D printing. *Heliyon*, **3**(10), 2017.

[3] G. Angelucci, F. Mollaioli, O. AlShawa. Evaluation of optimal lateral resisting systems for tall buildings subject to horizontal loads. *Procedia Manufacturing*, **44**, 457-464, 2020.

[4] G. Angelucci, S.M. Spence, F. Mollaioli. An integrated topology optimization framework for three-dimensional domains using shell elements. *The Structural Design of Tall and Special Buildings*, **30**(1), e1817., 2021.

[5] M. Zhu, Y. Yang, J.K. Guest, M.D. Shields. Topology optimization for linear stationary stochastic dynamics: applications to frame structures. *Structural Safety*, **67**, 116-131, 2017.

[6] G. Angelucci, G. Quaranta, F. Mollaioli. Energy-based topology optimization under stochastic seismic ground motion: Preliminary framework. *Energy-Based Seismic Engineering: Proceedings of IWEBSE*, 205–219, 2021.

[7] G. Angelucci, G. Quaranta, F. Mollaioli. Optimal lateral resisting systems for high-rise buildings under seismic excitation. *8th ECCOMAS thematic conference on computational methods in structural dynamics and earthquake engineering*, 2021.

[8] F. Gomez, B.F. Spencer. Topology optimization framework for structures subjected to stationary stochastic dynamic loads. *Structural and Multidisciplinary Optimization*, **59**, 813-833, 2019

[9] A. Y. Won, J. A. Pires, M. A. Haroun. Stochastic seismic performance evaluation of tuned liquid column dampers. *Earthquake Engineering & Structural Dynamics*, **25**(11), 1259-1274, 1996.

[10] J. Xu, B. F. Spencer, X. Lu, X. Chen, L. Lu. Optimization of structures subject to stochastic dynamic loading. *Computer-Aided Civil and Infrastructure Engineering*, **32**(8), 657-673, 2017.

[11] C. Su, B. Li, T. Chen, X. Dai. Stochastic optimal design of nonlinear viscous dampers for large-scale structures subjected to non-stationary seismic excitations based on dimension-reduced explicit method. *Engineering Structures*, **175**, 217-230, 2018.

[12] G. Angelucci, G. Quaranta, F. Mollaioli. Topology optimization of multi-story buildings under fully non-stationary stochastic seismic ground motion. *Structural and Multidisciplinary Optimization*, **65**(8), 217, 2022.

[13] Z. Liu, W. Liu, Y. Peng. Random function based spectral representation of stationary and non-stationary stochastic processes. *Probabilistic Engineering Mechanics,* **45**, 115–126, 2016.

[14] M.P. Bendsøe, O. Sigmund. Material interpolation schemes in topology optimization. *Archive of Applied Mechanics*, **69**(9), 635–654, 1999.

[15] F. Fan, G. Ahmadi. Nonstationary Kanai-Tajimi models for El Centro 1940 and Mexico city 1985 earthquakes. *Probabilistic Engineering Mechanics*, **5**(4):171–181, 1990.

[16] P.C. Jennings, G.W. Housner, C. Tsai. Simulated earthquake motions for design purposes. *4th world conference on earthquake engineering*, 1969.

[17] C.H. Yeh, Y. Wen. Modeling of nonstationary ground motion and analysis of inelastic structural response. *Structural Safety*, **8**(1–4):281–298, 1990.